SPE 56487

Analysis and Interpretation of Well Test Performance at Arun Field, Indonesia

T. Marhaendrajana, Texas A&M U., and N.J. Kaczorowski, Mobil Oil (Indonesia), and T.A. Blasingame, Texas A&M U.

This paper was prepared for presentation at the 1999 SPE Annual Technical Conference and Exhibition held in Houston, Texas, 3–6 October 1999.

Abstract

This paper presents a comprehensive field case history of the analysis and interpretation of all of the available well test data from the giant Arun Gas Field (Sumatra, Indonesia). Arun Field has estimated recoverable reserves on the order of 18-20 TCF and has 110 wells—78 producers, 11 injectors, 4 observation wells, and 17 abandoned. Approximately 100 well tests have been performed, and the analysis and interpretation of these data suggests strong existence of condensate accumulation near the wellbore as well as a "regional pressure decline" effect caused by competing production wells.

We demonstrate and discuss the analysis/interpretation techniques for wells that exhibit condensate banking and non-Darcy flow. We found that the 2-zone radial composite reservoir model is effective for diagnosing the effects of condensate banking at Arun Field.

We also demonstrate the development and application of a new solution for the analysis and interpretation for wells that exhibit "well interference" effects. Our new solution treats the "interference effect" as a regional pressure decline and this proposed solution accurately represents the well interference effects observed in many of the well tests obtained at Arun Field. Furthermore, this solution is shown to provide a much better interpretation of well test data from a multiwell reservoir system than the existing approaches–*i.e.*, assumption of no-flow or constant pressure boundaries, data truncation, etc.

Introduction

The objective for performing well test analysis at Arun Field is to provide information regarding flow properties (*e.g.* permeability, near-well skin factor, and the non-Darcy flow coefficient) as well as the radial extent of condensate banking around the wellbore. As the reservoir pressure at Arun Field has declined below the dew point (p_{dew}=4,200 psia), these data are quite valuable as an aid for estimating well deliverability and for assessing the need for well stimulation. Well test analyses are also useful for general reservoir management activities such as injection balancing and optimizing the performance of single and multiple wells.

For the analysis of well test data, we use the single-phase gas pseudopressure approach–as this method does not require knowledge of relative permeability data and it is much more convenient (and practical). The use of the single-phase pseudopressure approach is justified by the concept that most of the reservoir is (or at least until recently, was) at pressures above the dew point. Further, any multiphase pseudopressure approach will require knowledge of a representative relative permeability data set, as well as a pressure-saturation function that is used to relate pressure and mobility (*i.e.*, relative permeability).

The combined approach of using the single-phase gas pseudopressure coupled with a homogeneous reservoir model for the analysis well performance in gas condensate reservoir has been documented.[1-4] This particular approach yields an accurate estimate of *kh* (the permeability-thickness product)–however, the estimated skin factor is much higher than the actual (near-well) skin factor. This "high skin" phenomenon occurs because there is an accumulation of condensate liquid in the near-well region that behaves like second, lower permeability "reservoir" around the wellbore. To resolve this problem, a 2-zone radial composite reservoir model is used, where the inner zone represents the "condensate bank," and the outer zone represents the "dry gas reservoir." The application of the 2-zone radial composite reservoir model for the analysis of well test data from a gas condensate reservoir was demonstrated by Raghavan, *et al*,[3] and then by Yadavalli and Jones.[4]

We use the 2-zone radial composite reservoir model in our analysis if we observe a distinct inner zone (due to con-densate banking) in the well test data. This approach provides us with estimates of:

- Effective permeability to gas in both the "condensate bank," and in the "dry gas" reservoir,
- Mechanical skin factor,
- Radial extent of condensate banking,

In some (often many) cases, wellbore storage masks the inner region and affects our ability to obtain a complete suite of results. In such cases, we only obtain an estimate of the total skin factor. For the purpose of well stimulation (our objective is to

maximize well productivity), knowledge of the total skin factor is useful.

Another phenomenon that we have observed at Arun Field is the so-called "well interference" effect–which potentially leads us to misinterpret well test data. In fact, many of the well test cases taken at Arun Field show this behavior–this well interference effect tends to obscure the radial flow response, and hence, influence our analysis and interpretation efforts.

The first attempt to provide a generalized approach for the analysis of well test data from multiwell reservoir systems was presented by Onur *et.al.*[5] The application of their method is limited as it assumes that all of the wells in question produce at the same time and that the pseudosteady-state flow condition is achieved prior to shut-in. Arun Field has been produced for over 20 years and currently in "blowdown" mode–we can assume that the reservoir is at currently at pseudosteady-state flow conditions).

Drawdown and buildup tests induce local transient effects–which are controlled by the reservoir and near-well permeability, the skin factor, and the non-Darcy flow coefficient–but not the reservoir volume. Most of the well tests performed at Arun Field are relatively short (< 5 hours producing time), and the pseudosteady-state flow condition is not established in the area of investigation given such short production times.

To address this issue we have developed a new method for the analysis of well test data from a well in multiwell reservoir where we treat the "well interference" effect as a "Regional Pressure Decline." We note numerous cases of pressure buildup tests taken at Arun Field where the pressure actually declines at late times during the test–indicating communication with the surrounding wells that are still on production.

Our new approach employs a straight-line graphical analysis of data on a Cartesian plot ($\Delta t_e(d\Delta p/d\Delta t_e)$ versus $\Delta t^2/\Delta t_e$)–where this yields a direct estimation of permeability. We have called this the "well interference" plot. The multiwell model used to derived this approach also allows us to use type curve and semilog analysis–where "corrected" data functions are generated using the new "well interference" model proposed in the next section.

New Technique for the Analysis of Well Test Data in a Multiwell Reservoir System

Multiwell Model. In our new solution we assume a bounded homogeneous rectangular reservoir, with an arbitrary number of wells, positioned at arbitrary locations (as shown in Fig. 1). We also assume a single compressible fluid phase, but we allow any rate or pressure condition to be imposed at the well. However, our efforts in this work are focused on the constant flowrate case. The general analytical solution for the constant rate case is given by:

$$p_D(x_D,y_D,t_{DA}) = \sum_{i=1}^{n_{well}} q_{D,i}\, p_{D,i}(x_D,y_D,t_{DA},x_{wD,i},y_{wD,i})u(t_{DA}-t_{sDA,i}) \quad \text{.....(1)}$$

The derivation of Eq. 1 is given in Appendix A. This solution is valid for all flow regimes (*e.g.*, transient and boundary-dominated flow) and its computation is extremely rapid.

We have provided an extensive validation of this new solution using numerical simulation for the case of square reservoir with nine wells. For purposes of demonstration (not actual application), all wells are produced from the same starting time and produce at the same constant rate. The dimensionless pressure and pressure derivative functions from both the analytical and numerical solutions are plotted versus the dimensionless time function in **Fig. 2**. The open circles are the results from numerical simulation and the lines are the results from the new analytical solution. We note that these solutions are identical–which validates our new analytical solution, at least conceptually, as a mechanism to analyze well performance behavior in a multiwell reservoir system.

Regional Pressure Decline Model. To perform an analysis of well test data in a multiwell reservoir system, we must account for the "well interference" effects caused by offset production wells. Our approach is to consider this interference as a "Regional Pressure Decline," where this pressure drop acts uniformly in the area of investigation.

Our "well interference" model assumes that all of the wells in the reservoir are at pseudosteady-state flow conditions at the time the "focus" well is shut-in. After shut-in, the reservoir in the vicinity of the focus well will experience a significant pressure transient effect, but the offset wells remain on production. In simple terms, we assume that any rate change at the focus well (including a drawdown/buildup sequence) has little effect on the offset wells. However, these offset producing wells will eventually have a profound effect on the well performance at the focus well–including, as we noted from observations at Arun Field, the flattening and decline of a pressure buildup trend taken at the focus well.

The analytical solution for the focus well in this particular scenario is: (the details are provided in Appendix B)

$$p_{wD}(t_{DA}) = p_{D,1}([x_{wD,1}+\epsilon],[y_{wD,1}+\epsilon],t_{DA},x_{wD,1},y_{wD,1}) + 2\pi t_{DA}(a_D - 1) \quad \text{.....(2)}$$

where: $$a_D = \frac{V_p c_t}{q_1 B}\frac{d\bar{p}}{dt} = \frac{V_p c_t}{q_1 B}\alpha$$

Where: $\epsilon = r_{wD}/\sqrt{2}$ and $r_{wD} = r_w/\sqrt{A}$. $p_{D,1}(x_D,y_D,t_{DA},x_{wD,1},y_{wD,1})$ is the constant rate, single well solution for well 1 (*i.e.*, the focus well) and is given by Eq. A-4.

We have shown in Appendix C that the early-time pressure buildup equation (in $[p_{ws}\text{-}p_{wf}(\Delta t=0)]$ format) derived from Eq. 2 can be written as:

$$p_{sD}(\Delta t_{DA}) + 2\pi(a_D-1)\Delta t_{DA} = \frac{1}{2}\ln\left[\frac{4}{e^{\gamma}}\Delta t_{DAe}\frac{A}{r_w^2}\right] + s \quad \text{.....(3)}$$

Where Δt_{DAe} is given by:

$$\Delta t_{DAe} = \frac{\Delta t_{DA}\, t_{pDA}}{\Delta t_{DA} + t_{pDA}} \quad \text{.....(4)}$$

The derivative formulation of Eq. 3 is given by:

$$\Delta t_{DAe}\frac{d p_{sD}}{d\Delta t_{DAe}} = \frac{1}{2} - 2\pi(a_D-1)\frac{\Delta t_{DA}^2}{\Delta t_{DAe}} \quad \text{.....(5)}$$

Eq. 5 suggests that a Cartesian plot of $\Delta t_{DAe}(dp_{sD}/d\Delta t_{DAe})$ vs. $\Delta t_{DA}^2/\Delta t_{DAe}$ will form a straight-line trend. Furthermore, semilog plot of $p_{sD}+2\pi\Delta t_{DA}(a_D\text{-}1)$ versus Δt_{DAe} forms a straight line,

where this trend can be used to estimate formation permeability and skin factor.

To validate Eqs. 3 and 5, we use our new analytical solution (Eq. 1) for the case of a homogeneous, rectangular reservoir consisting of nine wells with a uniform well spacing (see inset schematic diagram in **Fig. 3**). Our focus well is the center well in this configuration. In this validation scenario, all wells except the focus well are put on production at the same time and at the same constant flowrate–are produced long enough to achieve pseudosteady-state flow conditions.

Once this occurs, the focus well is then put on production for various producing times to simulate various case of pressure drawdown (t_{pDA} = 10^{-5}, 10^{-4}, 10^{-3}, 10^{-2} respectively—where the dimensionless time in this comparison is based on total reservoir area). All of the other producing wells are left on production and the focus well is shut-in for a buildup test sequence. The case of single well in a reservoir of equal volume is also considered for comparison and discussion.

The pressure derivative responses for the focus well (for various producing times, t_p) are plotted for the pressure buildup cases using $\Delta t_{DA}(dp_{sD}/d\Delta t_{DA})$ versus Δt_{DA} as shown in **Fig. 3**. This plotting function was originally proposed by Onur *et.al*[5] as a means for estimating reservoir volume from a pressure buildup test. The data for the multiwell case are denoted by symbols and the data for the single well case are given by the solid lines.

We note that the data from the single well case approaches zero as shut-in time increases–this is a distinct characteristic of a "no-flow" boundary. On the other hand, the data from the multiwell case decrease linearly to negative values as shut-in time increases–*i.e.*, there is no "approaching zero" behavior. This behavior is an indication of "well interference," *i.e.*, the producing wells dominate the behavior of the reservoir system, and hence, the behavior of the "focus" well.

On **Figs. 4** and **5** we provide plots of the $\Delta t_{DAe}(dp_{sD}/d\Delta t_{DAe})$ function versus $\Delta t^2_{DA}/\Delta t_{DAe}$ as suggested by Eq. 5. These figures (**Fig. 4** is in semilog format, and **Fig. 5** is in Cartesian format) show that the data for the multiwell cases follow a straight line predicted by Eq. 5 (this is shown most clearly on **Fig. 5**). The slope of this line is proportional to the rate of change of the average reservoir pressure at the time of shut-in for the focus well.

For all cases, we note the general horizontal pressure derivative behavior (*i.e.*, the 0.5 line) as prescribed by Agarwal[6] for transient radial flow. The effect of the closed boundary (*i.e.*, the pressure derivative function decaying to zero) *is only apparent at very late times*. **Figs. 4** and **5** can be used as diagnostic tools to identify the effect of well interference on pressure buildup test behavior in a multiwell reservoir system.

Analysis Relations for Multiwell Reservoirs

We would like to develop a method for the analysis of pressure buildup test data from a well in a multiwell reservoir system that exhibits "well interference" effects. With that objective stated, we immediately note that Eq. 5 can be rearranged to obtain:

$$\Delta t_{DAe}\frac{d\,p_{sD}}{d\Delta t_{DAe}} + 2\pi(\alpha_D - 1)\frac{\Delta t^2_{DA}}{\Delta t_{DAe}} = \frac{1}{2} \quad \text{.....(6)}$$

We propose Eq. 6 as a new plotting function for the pressure derivative function–where this relation specifically accounts for the effects of well interference.

In **Fig. 6** we plot the various pressure derivative functions versus shut-in time or effective shut-in time. The solid lines denote the single well approach (including the well interference effects (there is no correction)) while the symbols denote the multiwell approach (correcting for the well interference effect as suggested by Eq. 6). We find that the multiwell approach yields a more clear (and longer) 0.5 line for the pressure derivative function.

In **Fig. 7**, we show that when we plot $p_{sD}+2\pi\Delta t_{DA}(\alpha_D-1)$ versus Δt_{DAe} on a semilog scale we obtain a much better semilog straight line trend than simply plotting p_{sD} versus Δt_{DAe}. This observation (as well as the general multiwell result (Eq. 6)), proves that we must take into account the effect of other producing wells in the analysis of pressure buildup test data in a multiwell reservoir system.

In Appendix C we provide Eqs. 3 and 5 in terms of field units. These results are given as:

$$p_{ws} + m_c\Delta t = p_{wf,\Delta t=0} + 162.6\frac{qB\mu}{kh}\times \left[\log(\Delta t_e) + \log\left[\frac{k}{\phi\mu c_t r_w^2}\right] - 3.22751 + 0.8686s\right] \quad \text{.....(7)}$$

$$\Delta t_e\frac{d\,p_{ws}}{d\Delta t_e} = 70.6\frac{qB\mu}{kh} - m_c\frac{\Delta t^2}{\Delta t_e} \quad \text{.....(8)}$$

where the "effective time" function is given by

$$\Delta t_e = \frac{t_p\Delta t}{(t_p+\Delta t)}$$

and the slope term is given by

$$m_c = 0.041665\frac{d\,\bar{p}}{dt}\frac{q}{q_{tot}}\left[\frac{q_{tot}}{q} - 1\right] \quad \text{.....(9)}$$

For the purpose of type curve matching using standard single-well type curves, we use the "corrected" pressure and pressure derivative functions from Eqs. 7 and 8. The functions are:

Pressure function:

$$p_{ws} + m_c\Delta t \quad \text{.....(10)}$$

Pressure derivative function:

$$\Delta t_e\frac{d\,p_{ws}}{d\Delta t_e} + m_c\frac{\Delta t^2}{\Delta t_e} \quad \text{.....(11)}$$

Analysis Procedures for Multiwell Reservoirs

To analyze pressure buildup tests taken in multiwell systems, we recommend the following procedures:

Step 1 Plot $\Delta t_e(dp_{ws}/d\Delta t_e)$ versus $\Delta t^2/\Delta t_e$ on a Cartesian scale. From the straight-line trend we obtain the slope m_c and intercept b_c. We calculate permeability using the intercept term as:

$$k = 70.6\frac{qB\mu}{b_c h} \quad \text{.....(12)}$$

Step 2 The Horner plot $[(p_{ws}+m_c\Delta t)$ versus $\log((t_p+\Delta t)/\Delta t)]$ can also be used to estimate formation properties. From the straight-line trend observed on the Horner plot, we

obtain the slope m_{sl} as well as the intercept term, $(p_{ws} + m_c \Delta t)_{\Delta t=1\text{hr}}$. Permeability is estimated using:

$$k = 162.6 \frac{qB\mu}{m_{sl} h} \quad \text{.....(13)}$$

And the skin factor is calculated using:

$$s = 1.1513 \left[\frac{(p_{ws} + m_c \Delta t)_{\Delta t=1\text{hr}} - p_{wf,\Delta t=0}}{m_{sl}} \right] - 1.1513 \left[\log\left[\frac{t_p}{t_p+1} \right] + \log\left[\frac{k}{\phi\mu c_t r_w^2} \right] - 3.22751 \right] \quad \text{.....(14)}$$

Step 3 In order to use standard single-well type curves for type curve matching, we must make the appropriate "corrections" given by Eqs. 10 and 11. These relations are:

Pressure function:

$$p_{ws} + m_c \Delta t \quad \text{.....(10)}$$

Pressure derivative function:

$$\Delta t_e \frac{d\, p_{ws}}{d\Delta t_e} + m_c \frac{\Delta t^2}{\Delta t_e} \quad \text{.....(11)}$$

Analysis of Pressure Buildup Test from Arun Field

In this section we discuss our analysis and interpretation of selected pressure buildup cases taken from the Arun Gas Field in Sumatra, Indonesia. We provide a wide range of examples, where the examples shown exhibit some type of "well interference" effects, as well as the effect of condensate banking (several cases).

Recall that we have analyzed and interpreted approximately 100 well tests from the Arun Field. Our goal is to identify cases that clearly illustrate certain types of behavior–in particular:

- Effects of non-Darcy flow (not as prevalent).
- Condensate banking (2-zone radial composite model).
- "Well interference"/boundary effects.

The following well test cases are presented:

- Well C-I-18 (A-096) [Test Date: 28 Sep 1992]
- Well C-II-15 (A-040) [Test Date: 26 May 1993]
- Well C-IV-11 (A-084) [Test Date: 05 Jan 1992]
- Well C-IV-11 (A-084) [Test Date: 04 May 1992]
- Well C-IV-16 (A-051) [Test Date: 16 Mar 1993]
- Well C-IV-16 (A-051) [Test Date: 16 Sep 1993]

Orientation for the Analysis/Interpretation Sequence:

Our analysis and interpretation of each well test case centers on the following plot sequence

Test Summary Plot–We use a log-log plot of the pseudopressure drop (Δp_p) and pseudopressure derivative ($\Delta p_p'$) functions versus the effective shut-in pseudotime function (Δt_{ae}). This plot includes the analysis results and the simulated test performance using these analysis results. The primary value of this plot is the visualization of the pseudopressure derivative function, and the corresponding flow regimes (and reservoir features) encountered during a test.

Horner Plot–We also use a "Horner" semilog plot of the shut-in pseudopressure function, p_{pws}, in order to provide the "conventional" semilog analysis of a particular data set. We typically provide the semilog trends for the "inner" and "outer" regions corresponding to the condensate and dry gas portions of the reservoir (respectively), for cases where both characteristics are observed.

Muskat Plot–The "Muskat" plot is a relatively new approach for establishing/confirming boundary-dominated flow behavior during a pressure buildup test sequence.[7] We use a Cartesian plot of the shut-in pseudopressure function, p_{pws}, versus the base derivative function, $dp_{pws}/\Delta t_a$. This plot provides an extrapolation to the average reservoir pressure (or in this case, pseudopressure), based on the principle that the pseudopressure and pseudopressure derivative functions are represented by a single term exponential function.

"Well Interference" Plot–The "well interference" plot is a new approach for verifying the "regional pressure decline" behavior associated with producing wells in a multiwell reservoir. This approach uses a Cartesian plot of the pseudopressure derivative ($\Delta p_p'$) function versus the shut-in pseudotime group ($\Delta t_a'/\Delta t_{ae}$). The slope of the resulting straight line (if a straight line exists) is used to "calibrate" the multiwell pressure and pressure derivative correction functions (Eqs. 10 and 11, respectively).

Well C-I-18 (A-096) [Test Date: 28 September 1992]. The corresponding figures showing our analysis for this case are provided in **Figs. 8** to **11**. Well C-I-18 (A-096) was completed in June 1991 and had an initial pressure of approximately 3173 psia at the time of completion. The results for this case are summarized in **Table 1**.

Test Summary Plot–**Fig. 8** clearly shows the condensate banking phenomena, as the pseudopressure derivative exhibits 2 distinct horizontal trends. The raw derivative data appear show a reservoir boundary, while the corrected derivative data show a continuance of the infinite-acting reservoir behavior (which is a result of our new multiwell correction function).

Horner Plot–**Fig. 9** verifies the condensate banking with a semilog straight line for the condensate bank as well as the dry gas portion of the reservoir. This plot also shows an apparent reservoir boundary at late times.

Muskat Plot–The Muskat plot provided in **Fig. 10** shows a reasonable straight-line trend at late times (to the left of the plot). However, this plot also shows a deviation from the expected linear trend at very late times, where this behavior prompts us to suggest that the nearby producing wells have caused a specific interference effect.

An argument could be made that the derivative function itself is the cause–as the derivative algorithm can skew the derivative values near the end-points. While plausible, we suggest that the nearby producing wells are the most likely cause of the "well interference" effects.

"Well Interference" Plot–**Fig. 11** exhibits a slightly scattered, but clearly linear trend. This observation validates our previous suggestion that deviation of the derivative function at late times is due to well interference from surrounding production wells. Our new multiwell reservoir model uniquely predicts this behavior.

Well C-II-15 (A-040) [Test Date: 26 May 1993]. Well C-II-15 (A-040) was completed in January 1981 and had an initial pressure of approximately 6444 psia at the time of completion. The results for this case are summarized in **Table 2**.

Test Summary Plot–In **Fig. 12**, the pseudopressure derivative function clearly shows the condensate banking phenomena, as well as a closed reservoir boundary (raw data). The corrected derivative data (although a bit scattered at very late times) suggests the continuation of the infinite-acting radial flow regime.

Horner Plot–In **Fig. 13** the shut-in pseudopressure function clearly indicates the presence of condensate banking (note the two semilog straight-line trends). The condensate bank feature appears to dominate most of the well performance behavior.

Muskat Plot–The Muskat plot in **Fig. 14** shows a relatively good linear trend at late times and tends to confirm the presence of a "closed boundary" feature.

"Well Interference" Plot–In **Fig. 15** we note a reasonably well defined linear trend, although there is considerable scatter at very late times. Using this trend, we find that the corrected functions in **Fig. 12** (the log-log plot) do suggest infinite-acting radial flow behavior.

Well C-IV-11 (A-084) [Test Date: 05 Jan 1992]. Well C-IV-11 (A-084) was completed in Arun Field in August 1990 and had an initial pressure of approximately 3835 psia at the time of completion. The results for this case are summarized in **Table 3**.

Test Summary Plot–**Fig. 16** provides a log-log plot of the pseudopressure functions where the effect of condensate banking is not obvious, but a large wellbore storage/skin factor "hump" is observed in the pseudopressure derivative function. As is typical at Arun Field, there does appear to be the influence of a closed reservoir boundary at very late times (uncorrected data).

Horner Plot–The Horner plot shown in **Fig. 17** gives a response that one would expect from a well in an infinite-acting homogeneous reservoir. There are no obvious/apparent features resembling condensate banking or reservoir boundaries.

Muskat Plot–The Muskat plot in **Fig. 18** exhibits a fairly well-defined linear trend at late times, confirming the presence of a "closed boundary" feature.

"Well Interference" Plot–In **Fig. 19** we observe a relatively consistent linear trend in the data, and conclude that well interference efforts are a possible mechanism. However, this trend only approaches zero, and does not actually extend to negative values, which is one criteria associated with the well interference model.

Well C-IV-11 (A-084) [Test Date: 04 May 1992]. This is another well test performed on Well C-IV-11 (A-084) on 4 May 1992 and the results for this case are summarized in **Table 4**. The purpose of this test was to evaluate the effectiveness of an acid fracturing treatment performed in January 1992.

Test Summary Plot–Comparing the log-log summary plot for this case (**Fig. 20**) with that of the previous test (**Fig. 16**), we immediately note a significantly smaller "hump" in the derivative function, suggesting that the well has been substantially stimulated. We note that the flowrate prior to this test is to the pre-stimulation test is about half that of the present test, but the maximum pseudopressure change at late times for the pre-stimulation test is almost twice that for the present test.

From **Fig. 20** we conclude that the effect of condensate banking is fairly modest, with only a slight "tail" in the pseudopressure derivative function. A boundary feature is apparent at very late times and the raw data again suggest that this is a closed boundary feature, while the "corrected" data indicate infinite-acting radial flow.

Horner Plot–We note two apparent semilog straight line trends on the Horner plot shown in **Fig. 21**. Both trends were constructed using the permeability values estimated for the "inner" (condensate) and "outer" (dry gas) regions. These trends appear to be reasonable, and should be considered accurate.

Muskat Plot–In **Fig. 22** we present the Muskat plot for this case and we note a very well-defined linear trend at late times, the extrapolated average reservoir pseudopressure ($\bar{p}_p$) is 1882.8 psia. For the pre-stimulation case, we obtained a $\bar{p}_p$ estimate of 1920.0 psia (**Fig. 18**).

"Well Interference" Plot–**Fig. 23** provides the "well interference" plot for this case. Comparing the trend on this plot with the pre-stimulation case (**Fig. 19**), we note a remarkable similarity in the estimated slopes of the data–confirming that the character of the regional pressure distribution has not changed significantly.

Well C-IV-16 (A-051) [Test Date: 16 Mar 1993]. Well C-IV-16 (A-051) was completed in Arun Field in March 1985 and had an initial pressure of approximately 5818 psia at the time of the original completion. This well was "sidetracked" and recompleted in mid-1989. The results for this case are provided in **Table 5**.

Test Summary Plot– In **Fig. 24** we present the summary log-log plot and we note a fairly well defined boundary feature. However, there are no obvious signs of conden-

sate banking–the estimated skin factor is low (0.62) and an excellent match of the data is obtained without using the 2-zone radial composite reservoir model.

Horner Plot–The Horner plot in **Fig. 25** shows the "classic" character of a pressure buildup test performed on a well in an infinite-acting homogeneous reservoir, with only wellbore storage and skin effects present. Only a very slight deviation of the pseudopressure trend is seen at late times, where this behavior is presumed to be a boundary effect.

Muskat Plot–In **Fig. 26** we present the Muskat plot for this case and we note an excellent straight-line trend at late times (as would be expected). However, we also note that the very last data deviate systematically from this trend, suggesting the possibility of external influences–*i.e.*, the well interference effect.

"Well Interference" Plot–In **Fig. 27** we immediately observe a new feature, the systematic deviation of the derivative trend. In fact, it appears that two linear trends could be constructed. We have elected to use the "earlier" trend as we have more confidence in these data (which are not influenced by "endpoint" effects in the derivative algorithm). However, either trend could be used, and perhaps an "average" trend should be used.

The point of this exercise is that we clearly observe the effects of well interference, but we have no single explanation for this behavior. For example, the drainage pattern may be non-uniform, and/or wells beyond the immediate vicinity could be affecting the pressure distribution in the area of the focus well.

Well C-IV-16 (A-051) [Test Date: 16 Sep 1993]. This is another well test performed on Well C-IV-16 (A-051) on 16 September 1993 and the results for this case are summarized in **Table 6**. This well test was performed to evaluate the effectiveness of an acid fracturing treatment performed in May 1993.

Test Summary Plot–From the early time data in **Fig. 28** we note a feature in the pseudopressure derivative function that appears to suggest fracture stimulation (or a least a significant improvement in near-well communication). This feature is not apparent in the previous test (see **Fig. 24**). The "raw" pressure derivative function in **Fig. 28** shows the apparent effect of a closed boundary at late times, while the "corrected" data suggest radial flow in an infinite-acting homogeneous reservoir.

Horner Plot–In **Fig. 29** we have the Horner plot for this case, where this particular plot does not provide any evidence of flow impediments, and suggests (at very late times) that a boundary has been encountered.

Muskat Plot–The Muskat plot for this case is shown in **Fig. 30** and we note a well-defined linear trend at late times, although we observe (as in the pre-stimulation test), that the last few points deviate systematically from the straight-line trend. The extrapolated average reservoir pseudopressure ($\bar{p}_p$) for this case is 1634.1 psia, while for the pre-stimulation case, we obtained a $\bar{p}_p$ estimate of 1788.3 psia (**Fig. 26**).

"Well Interference" Plot–In **Fig. 31** we present the "well interference" plot for this case and comparing the linear trend on this plot with the trend for the pre-stimulation case (**Fig. 27**), we find that the estimated slopes have changed considerably. However, given the somewhat ill-defined nature of the trends in both cases, we can only conclude qualitatively that the regional pressure distribution has changed.

Summary and Conclusions

In summary, we have developed a rigorous and coherent approach for the analysis of well test data taken from multiwell reservoir systems. Using the appropriate (dry gas) pseudopressure and pseudotime transformations, as well as the 2-zone radial composite reservoir model and the non-Darcy flow model, we have effectively analyzed all of the well test data taken from Arun Field.

We have also provided new insight into the effects of well interference in large multiwell reservoirs. The most innovative aspect of this work is the development of the new multiwell solution and corresponding analysis procedures. The most practical aspect of this work is the demonstration/validation of these multiwell analysis techniques for the majority of wells at Arun Field.

The following conclusions are derived from this work:

- The new "multiwell" solution has been successfully derived and applied for the analysis of well test data taken from a multiwell reservoir system.
- The appearance of "boundary" effects in pressure buildup test data taken in multiwell reservoirs can be corrected using our new approach. Care must be taken so as not to correct a true "closed boundary" effect.
- The 2-zone radial composite reservoir model has been shown to be representative for the analysis and interpretation of well test data from Arun Field (most wells exhibit radial composite reservoir behavior).
- The effect of non-Darcy flow on pressure buildup test analysis seems to be minor for the wells in Arun Field. Although not a focus of the present study, our analysis of the pressure drawdown (flow test) data appear to be much more affected by non-Darcy flow effects.

Nomenclature

A = Area, ft^2
B = Formation volume factor, RB/MSCF
c_t = Total compressibility, psi^{-1}
D = Non-Darcy Flow Coefficient, (MSCF/D)$^{-1}$
h = Thickness, ft
k = Formation permeability, md
p = Pressure or pseudopressure, psia
q = Sandface flow rate, MSCF/D
r_w = Wellbore radius, ft

s = Near-well skin factor, dimensionless
t = Time, hr
V_p = Pore volume
x = x-coordinate from origin, ft
y = y-coordinate from origin, ft
x_w = x-coordinate of well from origin, ft
y_w = y-coordinate of well from origin, ft
μ = Fluid viscosity, cp
ϕ = Porosity, fraction

Acknowledgements

We acknowledge the permission to publish field data provided by Pertamina and Mobil Oil Indonesia. We also acknowledge financial and technical support provided by Mobil E&P Technology Company (MEPTEC).

And finally, we acknowledge the technical, and computing support services provided by the Harold Vance Department of Petroleum Engineering at Texas A&M University.

References

1. Jones, J.R., Vo, D.T., and Raghavan, R.: "Interpretation of Pressure Buildup Responses in Gas Condensate Wells," *SPEFE* (March 1989).
2. Thompson, L.G., Niu, J.G., and Reynolds, A.C.: "Well Testing for Gas Condensate Reservoirs," paper SPE 25371 presented at the SPE Asia Pacific Oil & Gas Conference & Exhibition held in Singapore, 8-10 February 1993
3. Raghavan, R., Chu, W.C., Jones, J.R.: "Practical Consideration in the Analysis of Gas Condensate Well Tests," paper SPE 30576 presented at the SPE Annual Technical Conference & Exhibition held in Dallas, U.S.A., 22-25 October, 1995.
4. Yadavalli, S.K. and Jones, J.R.: "Interpretation of Pressure Transient Data from Hydraulically Fractured Gas Condensate," paper SPE 36556 presented at the 1996 SPE Annual Technical Conference and Exhibition held in Denver, Colorado, U.S.A., 6-9 October 1996.
5. Onur, M., Serra, K.V., and Reynolds, A.C.: "Analysis of Pressure Buildup Data Obtained at a Well located in a Multiwell System," *SPEFE* (March 1991) 101-110.
6. Agarwal, R.G.: "A New Method to Account for Producing Time Effects When Drawdown Type Curves Are Used to Analyze Pressure Buildup and Other Test Data," paper SPE 9289 presented at the 1980 SPE Annual Technical Conference and Exhibition, Dallas, Sept. 21-24.
7. Marhaendrajana, T. and Blasingame, T.A.: "Rigorous and Semi-Rigorous Approaches for the Evaluation of Average Reservoir Pressure from Pressure Transient Tests," paper SPE 38725 presented at the 1997 SPE Annual Technical Conference and Exhibition, San Antonio, TX, 5-8 October 1997.

Appendix A—Multiwell Solution

The mathematical model that describes the pressure behavior in a bounded rectangular reservoir with multiple wells producing at an arbitrary constant rate (**Fig.1**) is given by (Darcy units):

$$\frac{\partial^2 p}{\partial x^2}+\frac{\partial^2 p}{\partial y^2}-\sum_{i=1}^{n_{well}}\frac{q_i B}{Ah(k/\mu)}\delta(x-x_{w,i},y-y_{w,i})u(t-t_{s,i})=\frac{\phi\mu c_t}{k}\frac{\partial p}{\partial t} \quad \text{..... (A-1)}$$

In dimensionless variables, Eq.A-1 is written as:

$$\frac{\partial^2 p_D}{\partial x_D^2}+\frac{\partial^2 p_D}{\partial y_D^2}+2\pi\sum_{i=1}^{n_{well}}q_{D,i}\delta(x_D-x_{wD,i},y_D-y_{wD,i})u(t_{DA}-t_{sDA,i})=\frac{\partial p_D}{\partial t_{DA}} \quad \text{..... (A-2)}$$

where:

$$p_D=\frac{2\pi kh(p_i-p(x,y,t))}{q_{ref}B\mu}$$

$$t_{DA}=\frac{kt}{\phi\mu c_t A}$$

$$x_D=\frac{x}{\sqrt{A}}$$

$$y_D=\frac{y}{\sqrt{A}}$$

In Field units, these dimensionless variables are:

$$p_D=\frac{1}{141.2}\frac{kh(p_i-p(x,y,t))}{q_{ref}B\mu}$$

$$t_{DA}=0.0002637\frac{kt}{\phi\mu c_t A}$$

Eq. A-2 is solved analytically subject to the assumption of a no-flow condition at all reservoir boundaries (*i.e.*, this is a sealed ("no flow") boundary system). Following the work by Marhaendrajana and Blasingame[7] (1997), the solution of Eq. A-2 is:

$$p_D(x_D,y_D,t_{DA})=\sum_{i=1}^{n_{well}}q_{D,i}p_{D,i}(x_D,y_D,t_{DA},x_{wD,i},y_{wD,i})u(t_{DA}-t_{sDA,i}) \quad \text{..... (A-3)}$$

Where $p_{D,i}$ is the dimensionless pressure for the case of a single well in bounded reservoir produced at a constant rate.

From Ref. 7, the solution for a single well in a bounded rectangular reservoir produced at a constant rate is given as:

$$p_{D,i}(x_D,y_D,t_{DA},x_{wD,i},y_{wD,i})=\frac{1}{2}\sum_{m=-\infty}^{\infty}\sum_{n=-\infty}^{\infty}\left[E_1\left[\frac{(x_D+x_{wD,i}+2nx_{eD})^2+(y_D+y_{wD,i}+2my_{eD})^2}{4t_{DA}}\right]+E_1\left[\frac{(x_D-x_{wD,i}+2nx_{eD})^2+(y_D+y_{wD,i}+2my_{eD})^2}{4t_{DA}}\right]+E_1\left[\frac{(x_D+x_{wD,i}+2nx_{eD})^2+(y_D-y_{wD,i}+2my_{eD})^2}{4t_{DA}}\right]+E_1\left[\frac{(x_D-x_{wD,i}+2nx_{eD})^2+(y_D-y_{wD,i}+2my_{eD})^2}{4t_{DA}}\right]\right] \quad \text{..... (A-4)}$$

Although Eq. A-4 appears tedious, it is actually quite simple to compute and is remarkable efficient (*i.e.*, fast). When applying Eq. A-4, we use a convergence criteria of $1\text{x}10^{-20}$.

Appendix B—Regional Pressure Decline Model

In this Appendix we provide the development of the "regional pressure decline" model, where in this particular case, we utilize a complete multiwell solution, where this solution assumes that the surrounding production wells are at pseudosteady-state flow conditions.

This condition presumes that any rate change (*e.g.*, a pressure drawdown/buildup sequence) at the focus well will have very little effect on the surrounding production wells. Therefore, a pressure drawdown or pressure buildup test will cause transient flow conditions only in the vicinity of the focus well–not in the entire reservoir. Given the short period of a well test compared to the entire production history of the reservoir, this local transient phenomena is a reasonable and logical assumption.

Our new "regional pressure decline" model is written as follows (Darcy units):

$$\frac{\partial^2 p}{\partial x^2}+\frac{\partial^2 p}{\partial y^2}-\frac{q_1 B}{Ah(k/\phi)}\delta(x-x_{w,1},y-y_{w,1})-\sum_{i=2}^{n_{well}}\frac{q_i B}{Ah(k/\phi)}=\frac{\phi\mu c_t}{k}\frac{\partial p}{\partial t} \quad \text{.....(B-1)}$$

Writing Eq. B-1 in terms of dimensionless variables, we have

$$\frac{\partial^2 p_D}{\partial x_D^2}+\frac{\partial^2 p_D}{\partial y_D^2}+2\pi q_{D,1}\delta(x_D-x_{wD,1},y_D-y_{wD,1})+2\pi\sum_{i=2}^{n_{well}}q_{D,i}=\frac{\partial p_D}{\partial t_{DA}} \quad \text{.....(B-2)}$$

For the case of a no-flow outer boundary, the solution of Eq. B-2 is given as:

$$p_D(x_D,y_D,t_{DA})=p_{D,1}(x_D,y_D,t_{DA},x_{wD,1},y_{wD,1})+2\pi t_{DA}\sum_{i=2}^{n_{well}}q_{D,i} \quad \text{.....(B-3)}$$

Where $p_{D,1}(x_D,y_D,t_{DA},x_{wD,1},y_{wD,1})$ is the solution for the case of a single well in a bounded rectangular reservoir producing at a constant rate. This solution is given by Eq. A-4. Eq. B-3 is only strictly valid in the vicinity if the focus well (*i.e.*, well 1) and is used solely to model the pressure-time performance at the focus well.

From material balance, we have:

$$\frac{d\bar{p}}{dt}=\frac{q_{tot}B}{V_p c_t} \quad \text{.....(B-4)}$$

Defining a new parameter, the "well interference" coefficient, α_D, we obtain

$$\alpha_D=\frac{V_p c_t}{q_1 B}\frac{d\bar{p}}{dt}=\frac{V_p c_t}{q_1 B}\alpha \quad \text{.....(B-5)}$$

Substituting Eq. B-4 into Eq. B-3, and using the definition given by Eq. B-5, we obtain:

$$p_D(x_D,y_D,t_{DA})=p_{D,1}(x_D,y_D,t_{DA},x_{wD,1},y_{wD,1})+2\pi t_{DA}(\alpha_D-1) \quad \text{.....(B-6)}$$

The first term on right-hand-side of Eq. B-6 is the pressure response caused by well 1 (*i.e.*, the focus well), and the second term is the pressure response due to the other active producing wells in the reservoir system.

Evaluating the pressure response at the focus well, we have:

$$p_{wD}(t_{DA})=p_{D,1}([x_{wD,1}+\varepsilon],[y_{wD,1}+\varepsilon],t_{DA},x_{wD,1},y_{wD,1})+2\pi t_{DA}(\alpha_D-1) \quad \text{.....(B-7)}$$

where $\varepsilon=r_{wD}/\sqrt{2}$ and $r_{wD}=r_w/\sqrt{A}$.

Appendix C—Development of Pressure Buildup Analysis Method in Multiwell System

For a pressure buildup test performed on the focus well (*i.e.*, well 1) after a period of constant rate production in the focus well (with the surrounding production wells at pseudosteady-state flow conditions) the pressure at well 1 (*i.e.*, the focus well) is given by:

$$p_{wD}(t_{DA})=p_{D,1}([x_{wD,1}+\varepsilon],[y_{wD,1}+\varepsilon],t_{DA},x_{wD,1},y_{wD,1})-p_{D,1}([x_{wD,1}+\varepsilon],[y_{wD,1}+\varepsilon],t_{DA}-t_{pDA},x_{wD,1},y_{wD,1})+2\pi t_{DA}(\alpha_D-1) \quad \text{.....(C-1)}$$

From Eq. C-1, we can write the pressure buildup equation for well 1 (in $[p_i\text{-}p_{ws}]$ format) as:

$$\tilde{p}_{sD}(\Delta t_{DA})=p_{wD}(t_{pDA}+\Delta t_{DA})-p_{wD}(\Delta t_{DA})-p_{D,1}([x_{wD,1}+\varepsilon],[y_{wD,1}+\varepsilon],\Delta t_{DA},x_{wD,1},y_{wD,1})+2\pi(\alpha_D-1)(t_{pDA}+\Delta t_{DA}) \quad \text{.....(C-2)}$$

We would like to use the $[p_{ws}\text{-}p_{wf}(\Delta t=0)]$ format for our pressure buildup formulation, therefore we proceed as follows:

$$[p_{ws}-p_{wf}(\Delta t=0)]=[p_i-p_{wf}(\Delta t=0)]-[p_i-p_{ws}] \quad \text{.....(C-3)}$$

Hence,

$$p_{sD}(\Delta t_{DA})=p_{wD}(t_{pDA})-\tilde{p}_{sD}(\Delta t_{DA}) \quad \text{.....(C-4)}$$

Substituting Eqs. B-7 and C-2 into Eq. C-4, and rearranging, we obtain:

$$\begin{aligned}p_{sD}(\Delta t_{DA})=\;&p_{D,1}([x_{wD,1}+\varepsilon],[y_{wD,1}+\varepsilon],t_{pDA},x_{wD,1},y_{wD,1})\\&+2\pi(\alpha_D-1)t_{pDA}\\&-p_{D,1}([x_{wD,1}+\varepsilon],[y_{wD,1}+\varepsilon],t_{DA}+t_{pDA},x_{wD,1},y_{wD,1})\\&+p_{D,1}([x_{wD,1}+\varepsilon],[y_{wD,1}+\varepsilon],\Delta t_{DA},x_{wD,1},y_{wD,1})\\&-2\pi(\alpha_D-1)(t_{pDA}+\Delta t_{DA})\end{aligned} \quad \text{.....(C-5)}$$

Cancelling the similar terms, Eq. C-5 reduces to the following:

$$\begin{aligned}p_{sD}(\Delta t_{DA})=\;&p_{D,1}([x_{wD,1}+\varepsilon],[y_{wD,1}+\varepsilon],t_{pDA},x_{wD,1},y_{wD,1})\\&-p_{D,1}([x_{wD,1}+\varepsilon],[y_{wD,1}+\varepsilon],t_{DA}+t_{pDA},x_{wD,1},y_{wD,1})\\&+p_{D,1}([x_{wD,1}+\varepsilon],[y_{wD,1}+\varepsilon],\Delta t_{DA},x_{wD,1},y_{wD,1})\\&-2\pi(\alpha_D-1)\Delta t_{DA}\end{aligned} \quad \text{.....(C-6)}$$

Using Eq. A-4 for the $p_{D,1}$ variable, we have

$$\begin{aligned}p_{D,1}([x_{wD,1}+\varepsilon],[y_{wD,1}+\varepsilon],t_{DA},x_{wD,1},y_{wD,1})=\;&\frac{1}{2}\sum_{m=-\infty}^{\infty}\sum_{n=-\infty}^{\infty}E_1\left[\frac{(2x_{wD}+\varepsilon+2nx_{eD})^2+(2y_{wD}+\varepsilon+2my_{eD})^2}{4t_{DA}}\right]\\&+E_1\left[\frac{(\varepsilon+2nx_{eD})^2+(2y_{wD}+\varepsilon+2my_{eD})^2}{4t_{DA}}\right]\\&+E_1\left[\frac{(2x_{wD}+\varepsilon+2nx_{eD})^2+(\varepsilon+2my_{eD})^2}{4t_{DA}}\right]\\&+E_1\left[\frac{(\varepsilon+2nx_{eD})^2+(\varepsilon+2my_{eD})^2}{4t_{DA}}\right]\end{aligned} \quad \text{.....(C-7)}$$

The early time (*i.e.*, small Δt) approximation for Eq. C-7 is:

$$p_{D,1}([x_{wD,1}+\epsilon],[y_{wD,1}+\epsilon],t_{DA},x_{wD,1},y_{wD,1}) = \frac{1}{2}E_1\left[\frac{2\epsilon^2}{4t_{DA}}\right] \quad \text{.....(C-8)}$$

Inserting the definition of ϵ into Eq. C-8, we obtain

$$p_{D,1}([x_{wD,1}+\epsilon],[y_{wD,1}+\epsilon],t_{DA},x_{wD,1},y_{wD,1}) = \frac{1}{2}E_1\left[\frac{1}{4t_{DA}}\frac{r_w^2}{A}\right] \quad \text{.....(C-9)}$$

Substituting Eq. C-9 into Eq. C-6, we have

$$p_{sD}(\Delta t_{DA}) = \frac{1}{2}E_1\left[\frac{1}{4t_{pDA}}\frac{r_w^2}{A}\right] - \frac{1}{2}E_1\left[\frac{1}{4(t_{pDA}+\Delta t_{DA})}\frac{r_w^2}{A}\right] + \frac{1}{2}E_1\left[\frac{1}{4\Delta t_{DA}}\frac{r_w^2}{A}\right] - 2\pi(a_D-1)\Delta t_{DA} \quad \text{.....(C-10)}$$

Using the logarithmic approximation for the Exponential Integral terms, we write Eq. C-10 as:

$$p_{sD}(\Delta t_{DA}) = \frac{1}{2}\ln\left[\frac{4t_{pDA}}{e^{\gamma}}\frac{A}{r_w^2}\right] - \frac{1}{2}\ln\left[\frac{4(t_{pDA}+\Delta t_{DA})}{e^{\gamma}}\frac{A}{r_w^2}\right] + \frac{1}{2}\ln\left[\frac{4\Delta t_{DA}}{e^{\gamma}}\frac{A}{r_w^2}\right] - 2\pi(a_D-1)\Delta t_{DA} \quad \text{.....(C-11)}$$

Collecting the logarithm terms in Eq. C-11, we have

$$p_{sD}(\Delta t_{DA}) = \frac{1}{2}\ln\left[\frac{4}{e^{\gamma}}\frac{t_{pDA}\times\Delta t_{DA}}{(t_{pDA}+\Delta t_{DA})}\frac{A}{r_w^2}\right] - 2\pi(a_D-1)t_{DA} \quad \text{.....(C-12)}$$

Rearranging Eq. C-12 we obtain:

$$p_{sD}(\Delta t_{DA}) + 2\pi(a_D-1)\Delta t_{DA} = \frac{1}{2}\ln\left[\frac{4}{e^{\gamma}}\frac{t_{pDA}\times\Delta t_{DA}}{(t_{pDA}+\Delta t_{DA})}\frac{A}{r_w^2}\right] = \frac{1}{2}\ln\left[\frac{4}{e^{\gamma}}\Delta t_{DAe}\frac{A}{r_w^2}\right] \quad \text{.....(C-13)}$$

The Δt_{DAe} function is very similar to the "effective" shut-in time proposed by Agarwal.[6] The difference being that Δt_{DAe} is defined using dimensionless times based on the total drainage area, A.

$$\Delta t_{DAe} = \frac{t_{pDA}\times\Delta t_{DA}}{(t_{pDA}+\Delta t_{DA})}$$

This is an intermediate result, when we reduce these relations to field units, we will use the Agarwal effective shut-in time (Δt_e).

Including the near-well skin factor, Eq. C-13 becomes:

$$p_{sD}(\Delta t_{DA}) + 2\pi(a_D-1)\Delta t_{DA} = \frac{1}{2}\ln\left[\frac{4}{e^{\gamma}}\Delta t_{DAe}\frac{A}{r_w^2}\right] + s \quad \text{.....(C-14)}$$

Equation C-14 suggests that plot of $p_{sD}+2\pi\Delta t_{DA}(a_D-1)$ versus $\log(\Delta t_{DAe})$ will form a straight line. Substituting the definition of the dimensionless variables (in terms of field units) into Eq. C-14, we obtain

$$\frac{1}{141.2}\frac{kh(p_{ws}-p_{wf,\Delta t=0})}{qB\mu} + 2\pi\frac{0.0002637k\Delta t}{\phi\mu c_t A}\left[\frac{q_{tot}}{q}-1\right] = \frac{1}{2}\ln\left[\frac{4}{e^{\gamma}}\frac{0.0002637k}{\phi\mu c_t r_w^2}\frac{t_p\Delta}{(t\ +\Delta)}\right] + \quad \text{.....(C-15)}$$

Multiplying both sides of Eq. C-15 by $141.2qB\mu/kh$ and substituting the material balance relation, $d\bar{p}/dt = 5.615q_{tot}B/\phi hAc_t$, we have

$$p_{ws} + 0.041665\frac{d\bar{p}}{dt}\frac{q}{q_{tot}}\left[\frac{q_{tot}}{q}-1\right]\Delta t = p_{wf,\Delta t=0} + 162.6\frac{qB\mu}{kh}\times\left[\log\left[\frac{t_p\Delta t}{(t_p+\Delta t)}\right] + \log\left[\frac{k}{\phi\mu c_t r_w^2}\right] - 3.22751 + 0.8686s\right] \quad \text{..... (C-16)}$$

To determine coefficient of Δt on the left-hand-side of Eq. C-16, we proceed by differentiating Eq. C-14 with respect to Δt_{DA}, which gives us the following result

$$\Delta t_{DA}\frac{dp_{sD}}{d\Delta t_{DA}} = \frac{1}{2}\frac{t_{pDA}}{(t_{pDA}+\Delta t_{DA})} - 2\pi\Delta t_{DA}(a_D-1) \quad \text{..... (C-17)}$$

Multiplying both sides by $\frac{(t_{pDA}+\Delta t_{DA})}{t_{pDA}}$, we obtain

$$\frac{(t_{pDA}+\Delta t_{DA})}{t_{pDA}}\Delta t_{DA}\frac{dp_{sD}}{d\Delta t_{DA}} = \frac{1}{2} - 2\pi(a_D-1)\frac{(t_{pDA}+\Delta t_{DA})}{t_{pDA}}\Delta t_{DA} \quad \text{..... (C-18)}$$

Using the following identity in terms of Δt_{DA} and Δt_{DAe}, we have

$$\Delta t_{DAe}\frac{dp_{sD}}{d\Delta t_{DAe}} = \frac{t_{pDA}\Delta t_{DA}}{(t_{pDA}+\Delta t_{DA})}\frac{dp_{sD}}{d\Delta t_{DA}}\frac{d\Delta t_{DA}}{d\Delta t_{DAe}} = \frac{t_{pDA}\Delta t_{DA}}{(t_{pDA}+\Delta t_{DA})}\frac{dp_{sD}}{d\Delta t_{DA}}\left[\frac{(t_{pDA}+\Delta t_{DA})}{t_{pDA}}\right]^2 = \frac{(t_{pDA}+\Delta t_{DA})}{t_{pDA}}\Delta t_{DA}\frac{dp_{sD}}{d\Delta t_{DA}} \quad \text{..... (C-19)}$$

Substituting Eq. C-19 in Eq. C-18, we obtain

$$\Delta t_{DAe}\frac{dp_{sD}}{d\Delta t_{DAe}} = \frac{1}{2} - 2\pi(a_D-1)\frac{(t_{pDA}+\Delta t_{DA})}{t_{pDA}}\Delta t_{DA}$$

or finally, we have

$$\Delta t_{DAe}\frac{dp_{sD}}{d\Delta t_{DAe}} = \frac{1}{2} - 2\pi(a_D-1)\frac{\Delta t_{DA}^2}{\Delta t_{DAe}} \quad \text{..... (C-20)}$$

Eq. C-20 suggests that a plot of $\Delta t_{DAe}(dp_{sD}/d\Delta t_{DAe})$ versus the $\Delta t_{DA}^2/\Delta t_{DAe}$ group will form a straight-line trend. Rearranging Eq. C-20 further, we obtain

$$\Delta t_{DAe}\frac{dp_{sD}}{d\Delta t_{DAe}} + 2\pi(a_D-1)\frac{\Delta t_{DA}^2}{\Delta t_{DAe}} = \frac{1}{2} \quad \text{..... (C-21)}$$

Substituting the definition of the appropriate dimensionless variables (in terms of field units) into Eq. C-20, we have

$$\Delta t_e\frac{dp_{ws}}{d\Delta t_e} = 70.6\frac{qB\mu}{kh} - 0.041665\frac{d\bar{p}}{dt}\frac{q}{q_{tot}}\left[\frac{q_{tot}}{q}-1\right]\frac{\Delta t^2}{\Delta t_e} \quad \text{..... (C-22)}$$

From Eq. C-22, we can define the slope term, m_c, as

$$m_c = 0.041665\frac{d\bar{p}}{dt}\frac{q}{q_{tot}}\left[\frac{q_{tot}}{q}-1\right] \quad \text{..... (C-23)}$$

Therefore, we can now write Eq. C-22 as follows

$$\Delta t_e \frac{d\,p_{ws}}{d\,\Delta t_e} = 70.6\frac{qB\mu}{kh} - m_c\frac{\Delta t^2}{\Delta t_e} \quad \text{.....(C-24)}$$

Equation C-24 suggests that plot of $\Delta t_e(dp_{ws}/d\Delta t_e)$ versus $\Delta t^2/\Delta t_e$ will form a straight-line trend with a slope m_c and an intercept $70.6qB\mu/(kh)$—where we define the intercept term as b_c. We can calculate formation permeability using

$$k = 70.6\frac{qB\mu}{b_c h} \quad \text{.....(C-25)}$$

Recalling Eq. C-16, we have

$$p_{ws} + 0.041665\frac{d\,\bar{p}}{dt}\frac{q}{q_{tot}}\left[\frac{q_{tot}}{q} - 1\right]\Delta t = p_{wf,\Delta t=0} + 162.6\frac{qB\mu}{kh}\times \left[\log\left[\frac{t_p\Delta t}{(t_p+\Delta t)}\right] + \log\left[\frac{k}{\phi\mu c_t r_w^2}\right] - 3.22751 + 0.8686s\right] \quad \text{.....(C-16)}$$

Substituting Eq. C-23 into Eq. C-16 gives us:

$$p_{ws} + m_c\Delta t = p_{wf,\Delta t=0} + 162.6\frac{qB\mu}{kh}\times \left[\log(\Delta t_e) + \log\left[\frac{k}{\phi\mu c_t r_w^2}\right] - 3.22751 + 0.8686s\right] \quad \text{...(C-26)}$$

where effective time is given by

$$\Delta t_e = \frac{t_p\Delta t}{(t_p+\Delta t)}$$

Eq. C-26 suggests that a plot of $(p_{ws}+m_c\Delta t)$ vs. $\log(\Delta t_e)$ will yield a straight line from which we can determine permeability (from the slope term) and skin factor (from the intercept term). The coefficient m_c is obtained from a Cartesian plot of $\Delta t_e(dp_{ws}/d\Delta t_e)$ versus $\Delta t^2/\Delta t_e$.

Using this approach, one can construct an appropriate semilog plot for a well undergoing a pressure buildup test in a multiwell reservoir system. In fact, the $p_{ws}+m_c\Delta t$ data function can also be used in the conventional Horner plot format [*i.e.*, $p_{ws}+m_c\Delta t$ versus $\log((t_p+\Delta t)/\Delta t)$].

The formation permeability and near-well skin factor are calculated using the following relations (respectively):

$$k = 162.6\frac{qB\mu}{m_{sl}h} \quad \text{.....(C-27)}$$

$$s = 1.1513\left[\frac{(p_{ws}+m_c\Delta t)_{\Delta t=1\text{hr}} - p_{wf,\Delta t=0}}{m_{sl}}\right] - 1.1513\left[\log\left[\frac{t_p}{t_p+1}\right] + \log\left[\frac{k}{\phi\mu c_t r_w^2}\right] - 3.22751\right] \quad \text{.....(C-28)}$$

where m_{sl} is the slope of the straight-line trend on a semilog plot [*i.e.*, $(p_{ws}+m_c\Delta t)$ versus $\log(\Delta t_e)$ (Agarwal format) or $p_{ws}+m_c\Delta t$ versus $\log((t_p+\Delta t)/\Delta t)$ (Horner Format)].

For the purpose of performing type curve analysis using the standard single-well type curves, we must use the corrected pressure and pressure derivative functions which are derived from Eq. C-24 and Eq. C-26. These "correction" functions are:

Pressure function:

$$p_{ws} + m_c\Delta t \quad \text{.....(C-29)}$$

Pressure derivative function:

$$\Delta t_e\frac{d\,p_{ws}}{d\,\Delta t_e} + m_c\frac{\Delta t^2}{\Delta t_e} \quad \text{.....(C-30)}$$

TABLE 1—SUMMARY OF ANALYSIS FOR WELL C-I-18 (A-096) [TEST DATE: 28 SEPTEMBER 1992]

Parameter	Cartesian Plot	Horner Plot	Log-log Plot	Muskat Plot
Inner zone permeability k_1, md	---	7.36	7.36	---
Outer zone permeability k_2, md	15.3	15.3	15.3	---
Near-well skin factor, s	---	0.68	0.129	---
Total skin factor, s_t	---	4.55	---	---
Non-Darcy flow coeff. D, $(\text{MSCF/D})^{-1}$	---	---	$5\text{x}10^{-6}$	---
Inner zone radius, r_i, ft	---	---	19	---
Average reservoir pseudo-pressure $\bar{p}_p$, psia	---	---	---	1148.6

TABLE 2—SUMMARY OF ANALYSIS FOR WELL C-II-15 (A-040) [TEST DATE: 26 MAY 1993]

Parameter	Cartesian Plot	Horner Plot	Log-log Plot	Muskat Plot
Inner zone permeability k_1, md	---	7.20	7.20	---
Outer zone permeability k_2, md	61.4	61.4	61.4	---
Near-well skin factor, s	---	-0.138	-0.707	---
Total skin factor, s_t	---	28.1	---	---
Non-Darcy flow coeff. D, $(\text{MSCF/D})^{-1}$	---	---	$1.6\text{x}10^{-5}$	---
Inner zone radius, r_i, ft	---	---	21	---
Average reservoir pseudo-pressure $\bar{p}_p$, psia	---	---	---	1132.8

TABLE 3—SUMMARY OF ANALYSIS FOR WELL C-IV-11 (A-084) [TEST DATE: 5 JANUARY 1992]

Parameter	Cartesian Plot	Horner Plot	Log-log Plot	Muskat Plot
Inner zone permeability k_1, md	---	---	---	---
Outer zone permeability k_2, md	6.04	6.04	6.04	---
Near-well skin factor, s	---	---	---	---
Total skin factor, s_t	---	33.5	33.5	---
Non-Darcy flow coeff. D, $(\text{MSCF/D})^{-1}$	---	---	---	---
Inner zone radius, r_i, ft	---	---	---	---
Average reservoir pseudo-pressure $\bar{p}_p$, psia	---	---	---	1920

TABLE 4—SUMMARY OF ANALYSIS FOR WELL C-IV-11 (A-084) [TEST DATE: 4 MAY 1992]

Parameter	Cartesian Plot	Horner Plot	Log-log Plot	Muskat Plot
Inner zone permeability k_1, md	---	1.06	1.06	---
Outer zone permeability k_2, md	6.25	6.25	6.25	---
Near-well skin factor, s	---	-1.57	-1.54	---
Total skin factor, s_t	---	7.85	---	---
Non-Darcy flow coeff. D, (MSCF/D)$^{-1}$	---	---	---	---
Inner zone radius, r_i, ft	---	---	9	---
Average reservoir pseudo-pressure $\bar{p}_p$, psia	---	---	---	1883

TABLE 5—SUMMARY OF ANALYSIS FOR WELL C-IV-16 (A-051) [TEST DATE: 16 MARCH 1993]

Parameter	Cartesian Plot	Horner Plot	Log-log Plot	Muskat Plot
Inner zone permeability k_1, md	---	---	---	---
Outer zone permeability k_2, md	0.972	0.972	0.972	---
Near-well skin factor, s	---	---	---	---
Total skin factor, s_t	---	0.56	0.62	---
Non-Darcy flow coeff. D, (MSCF/D)$^{-1}$	---	---	---	---
Inner zone radius, r_i, ft	---	---	---	---
Average reservoir pseudo-pressure $\bar{p}_p$, psia	---	---	---	1788.3

TABLE 6—SUMMARY OF ANALYSIS FOR WELL C-IV-16 (A-051) [TEST DATE: 16 SEPTEMBER 1993]

Parameter	Cartesian Plot	Horner Plot	Log-log Plot	Muskat Plot
Inner zone permeability k_1, md	---	---	---	---
Outer zone permeability k_2, md	1.97	1.97	1.97	---
Near-well skin factor, s	---	---	---	---
Total skin factor, s_t	---	-1.3	-1.2	---
Non-Darcy flow coeff. D, (MSCF/D)$^{-1}$	---	---	---	---
Inner zone radius, r_i, ft	---	---	---	---
Average reservoir pseudo-pressure $\bar{p}_p$, psia	---	---	---	1634.1

Well/Reservoir Configuration

-Bounded rectangular reservoir with constant thickness.
-Wells are fully penetrating.
-Well locations are arbitrary.

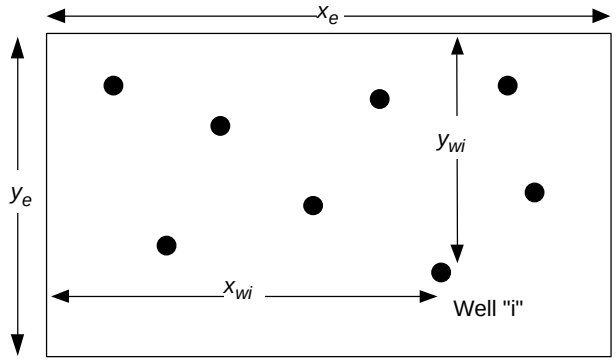

Fig. 1—Schematic diagram of the multiwell reservoir model.

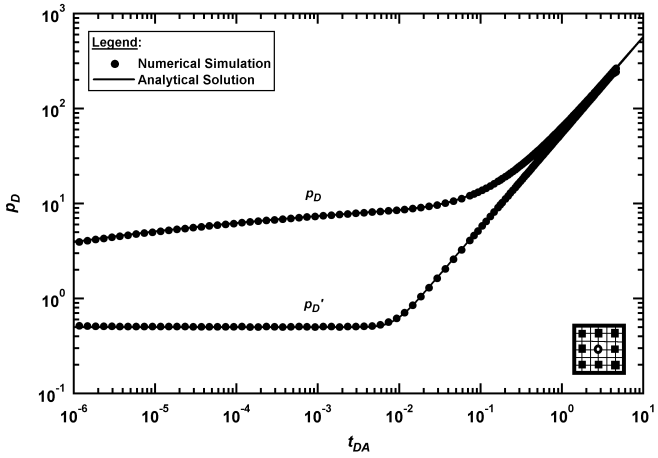

Fig. 2—Dimensionless pressure and pressure derivative functions versus dimensionless time–comparison of analytical and numerical solutions.

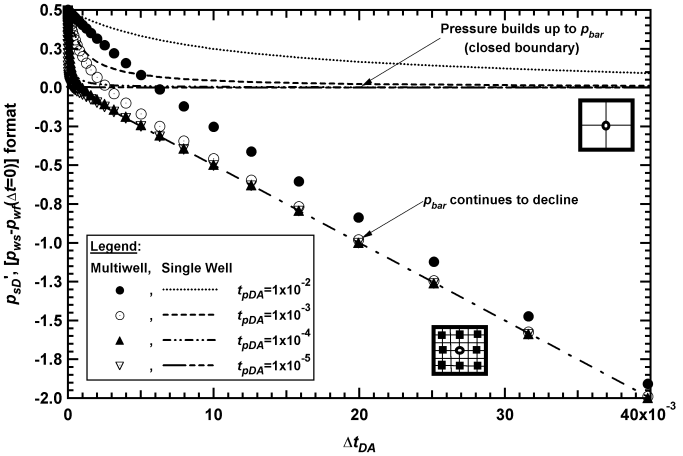

Fig. 3—Cartesian plot of dimensionless pressure derivative functions versus dimensionless shut-in time functions.

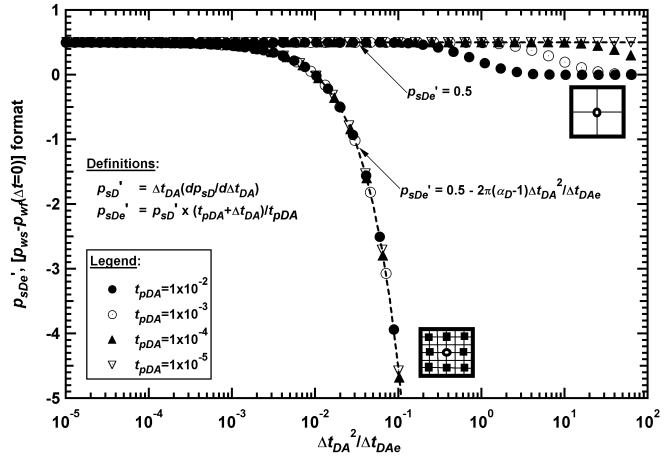

Fig. 4—Semilog plot of dimensionless pressure derivative functions versus dimensionless shut-in time functions (new plotting functions).

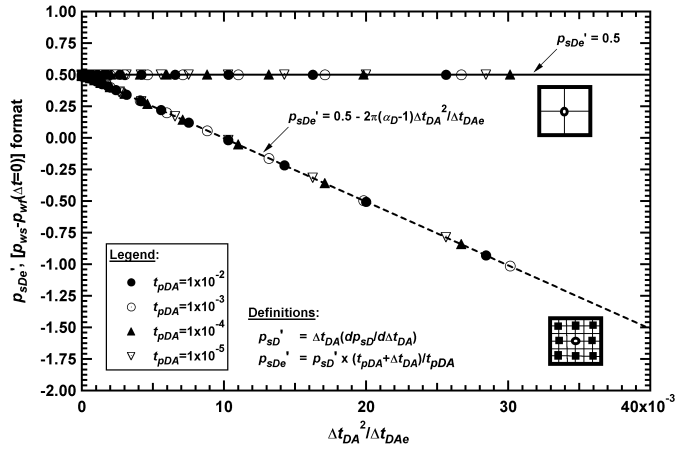

Fig. 5—Cartesian plot of dimensionless pressure derivative functions versus dimensionless shut-in time functions (new plotting functions).

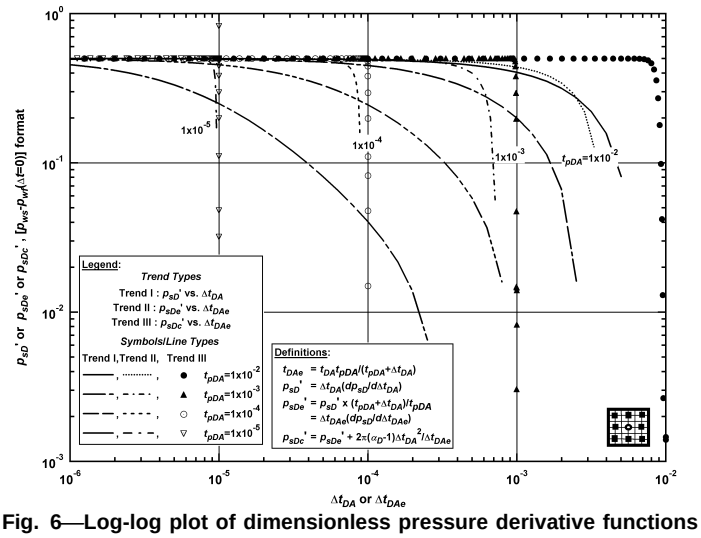

Fig. 6—Log-log plot of dimensionless pressure derivative functions versus dimensionless shut-in time functions (multiwell model).

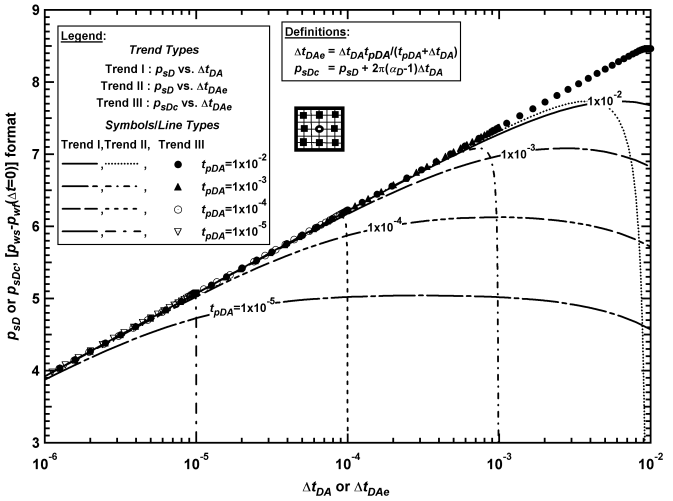

Fig. 7—Semi-log plot of dimensionless pressure functions versus dimensionless shut-in time functions (multiwell model).

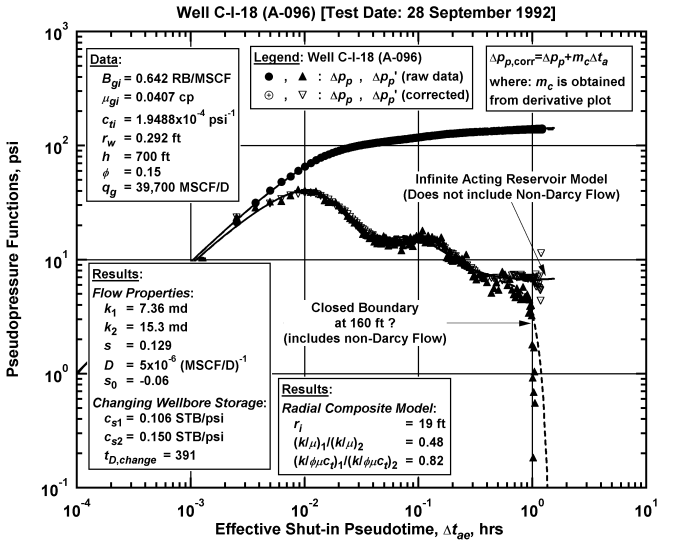

Fig. 8—Log-log plot of shut-in pseudopressure functions versus effective shut-in pseudotime for Well C-I-18 (A-096).

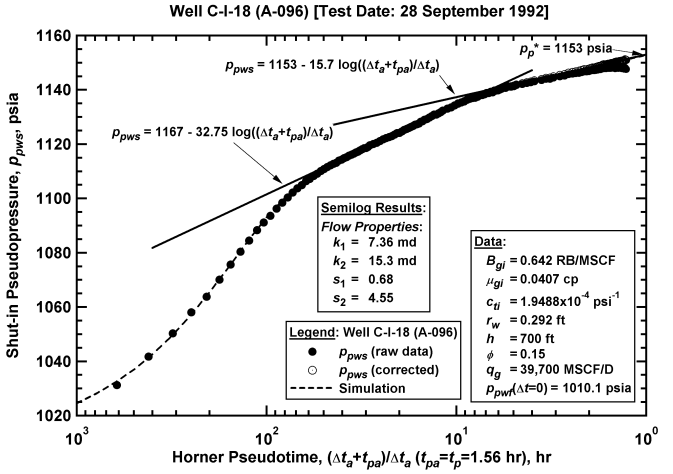

Fig. 9—Semilog plot of shut-in pseudopressure function versus Horner pseudotime for Well C-I-18 (A-096).

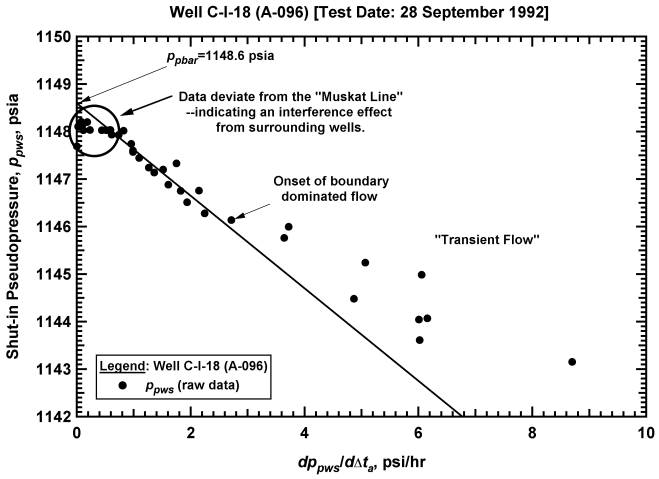

Fig. 10—Muskat plot for Well C-I-18 (A-096).

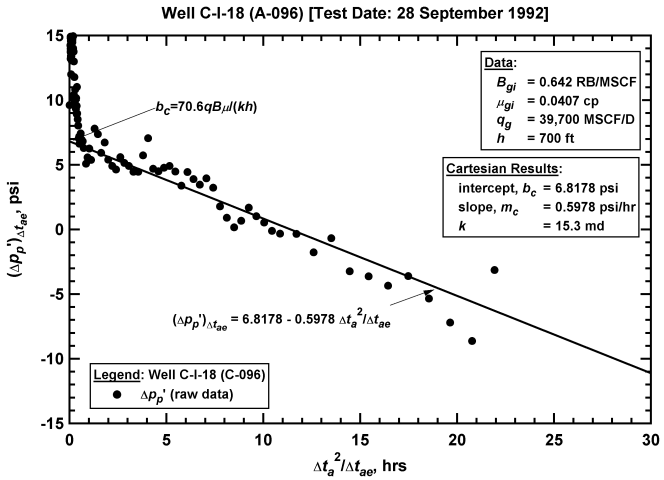

Fig. 11—Well Interference plot for Well C-I-18 (A-096).

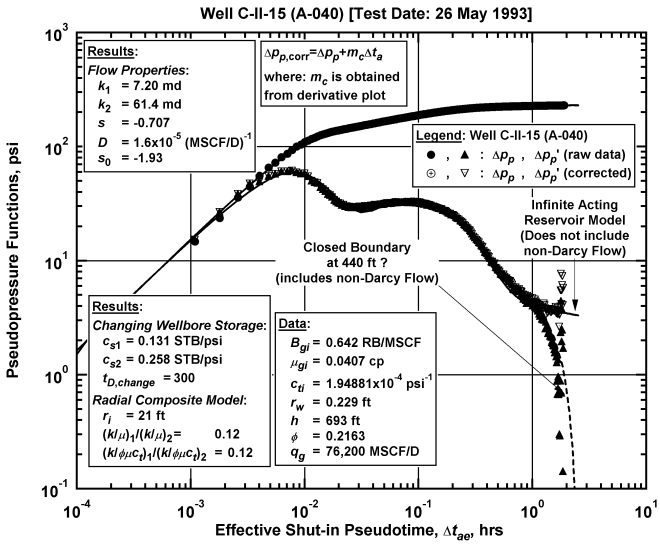

Fig. 12—Log-log plot of shut-in pseudopressure functions versus effective shut-in pseudotime for Well C-II-15 (A-040).

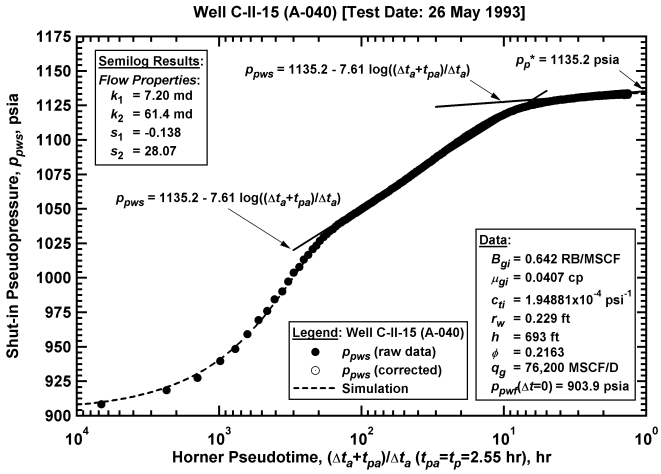

Fig. 13—Semilog plot of shut-in pseudopressure function versus Horner pseudotime for Well C-II-15 (A-040).

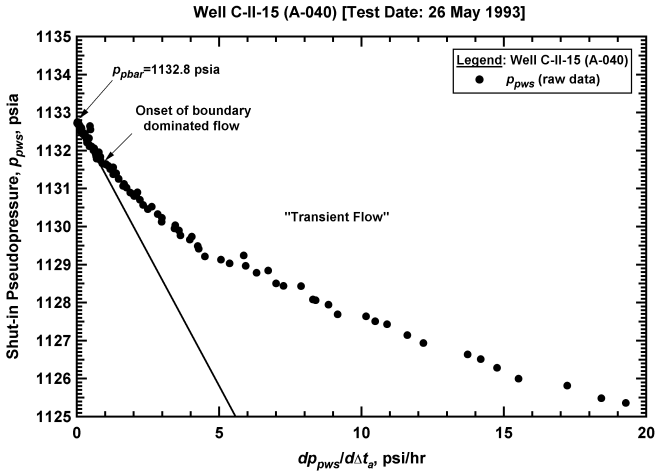

Fig. 14—Muskat plot for Well C-II-15 (A-040).

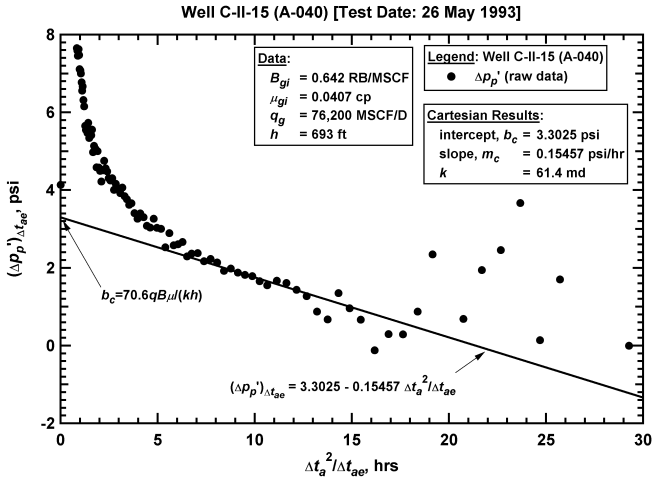

Fig. 15—Well Interference plot for Well C-II-15 (A-040).

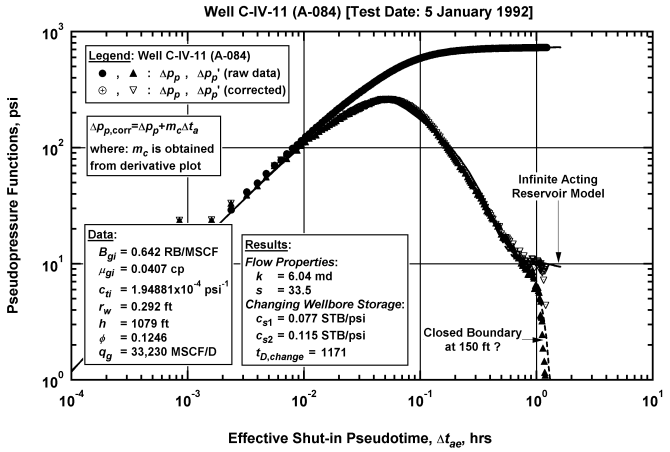

Fig. 16—Log-log plot of shut-in pseudopressure functions versus effective shut-in pseudotime for Well C-IV-11 (A-084) [5 January 1992].

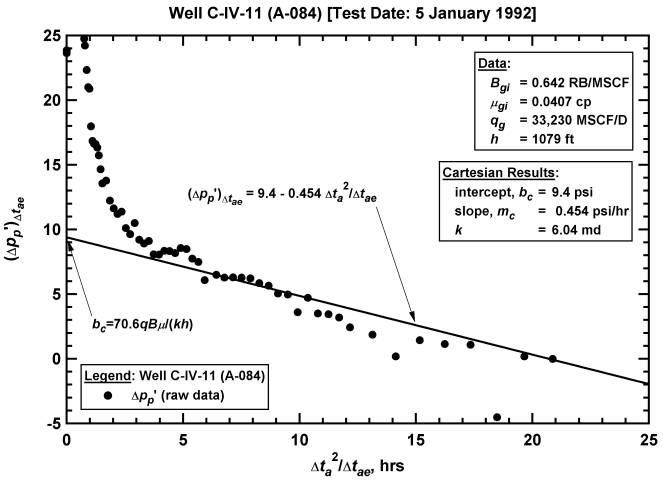

Fig. 19—Well Interference plot for Well C-IV-11 (A-084) [5 Jan 1992].

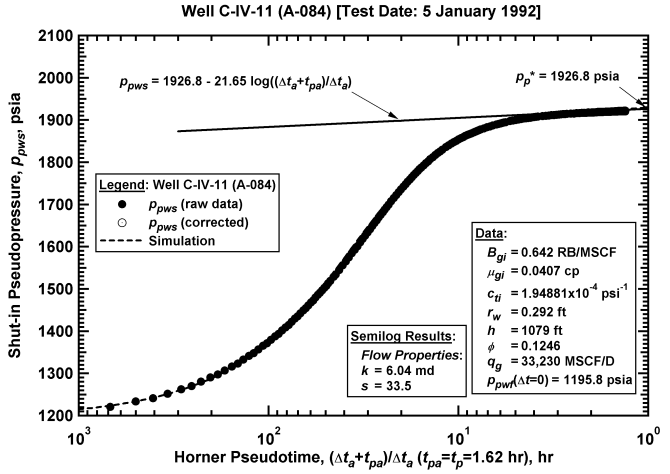

Fig. 17—Semilog plot of shut-in pseudopressure function versus Horner pseudotime for Well C-IV-11 (A-084) [5 January 1992].

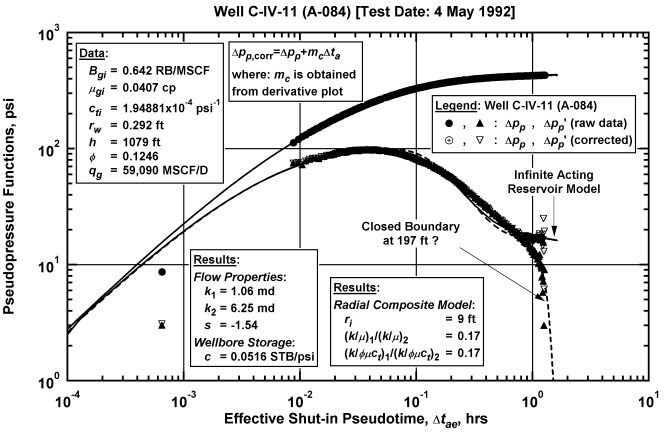

Fig. 20—Log-log plot of shut-in pseudopressure functions versus effective shut-in pseudotime for Well C-IV-11 (A-084) [4 May 1992].

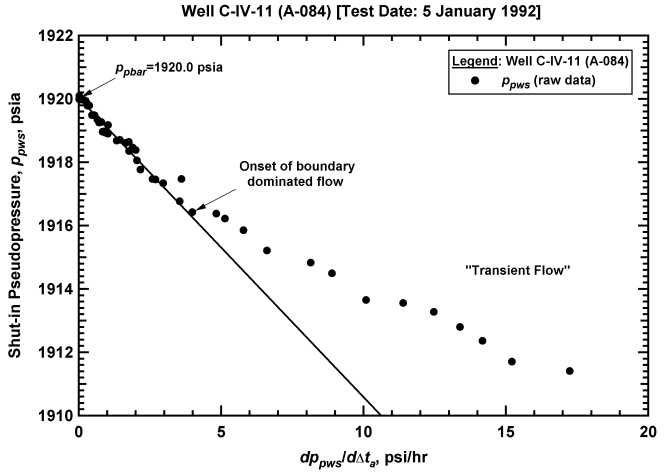

Fig. 18—Muskat plot for Well C-IV-11 (A-084) [5 January 1992].

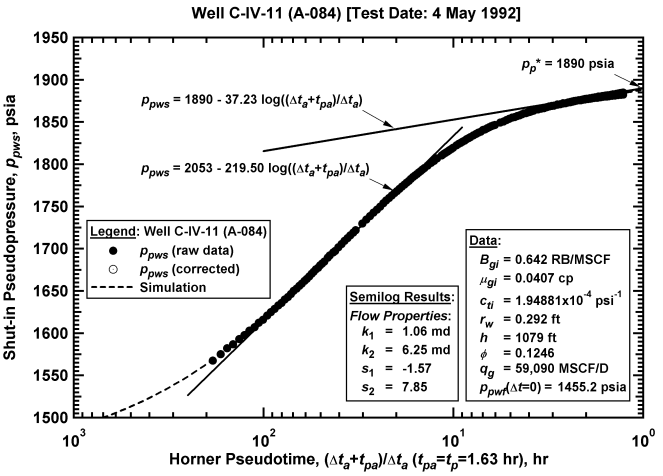

Fig. 21—Semilog plot of shut-in pseudopressure function versus Horner pseudotime for Well C-IV-11 (A-084) [4 May 1992].

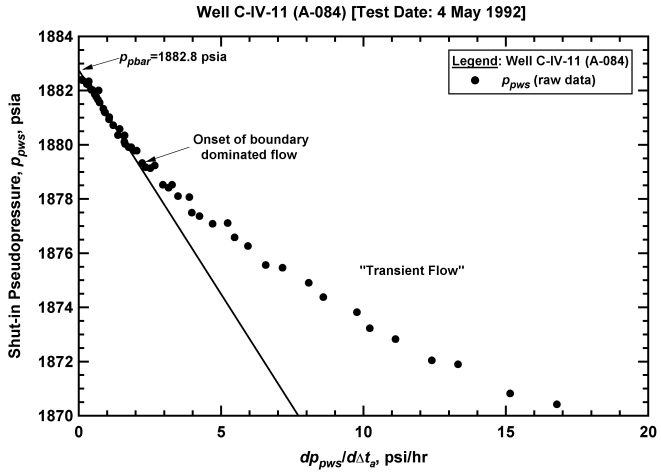

Fig. 22—Muskat plot for Well C-IV-11 (A-084) [4 May 1992].

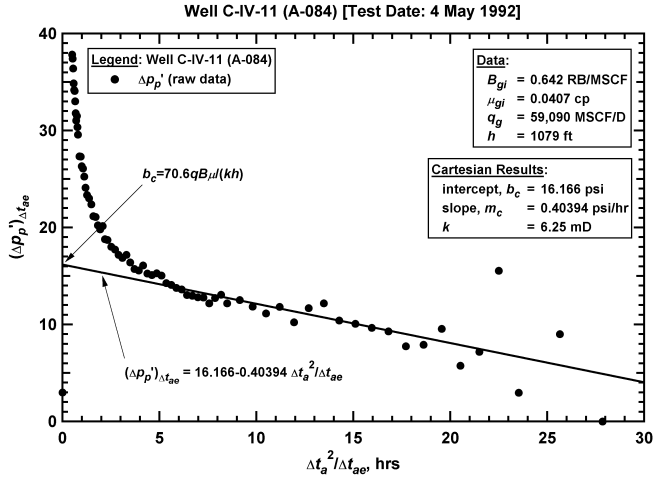

Fig. 23—Well Interference plot for Well C-IV-11 (A-084) [4 May 1992].

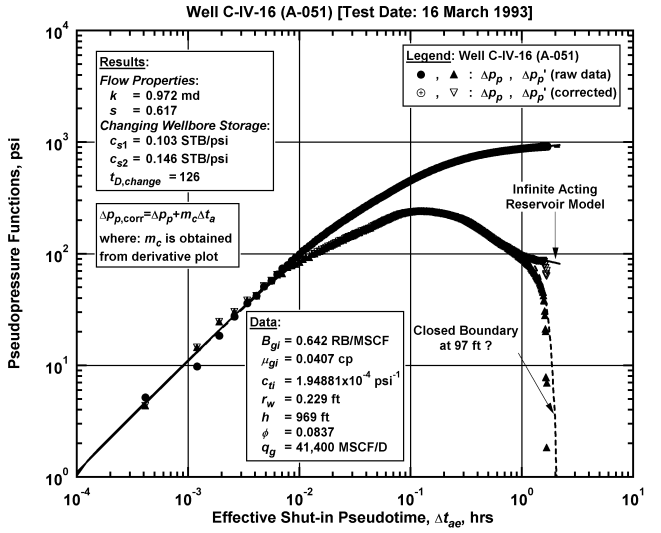

Fig. 24—Log-log plot of shut-in pseudopressure functions versus effective shut-in pseudotime for Well C-IV-16 (A-051) [16 March 1993].

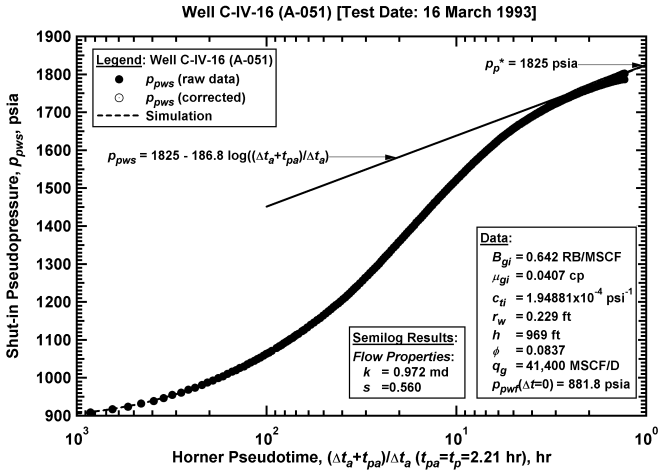

Fig. 25—Semilog plot of shut-in pseudopressure function versus Horner pseudotime for Well C-IV-16 (A-051) [16 March 1993].

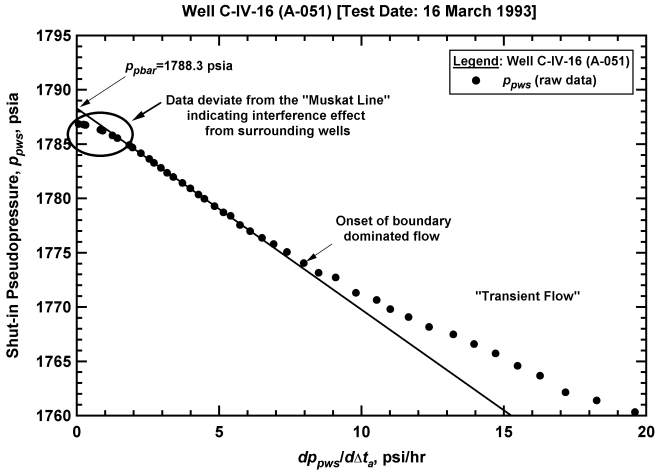

Fig. 26—Muskat plot for Well C-IV-16 (A-051) [16 March 1993].

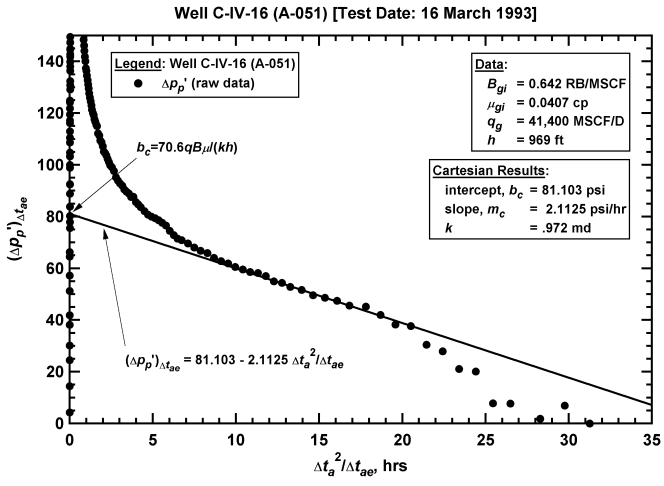

Fig. 27—Well Interference plot, Well C-IV-16 (A-051) [16 Mar 1993].

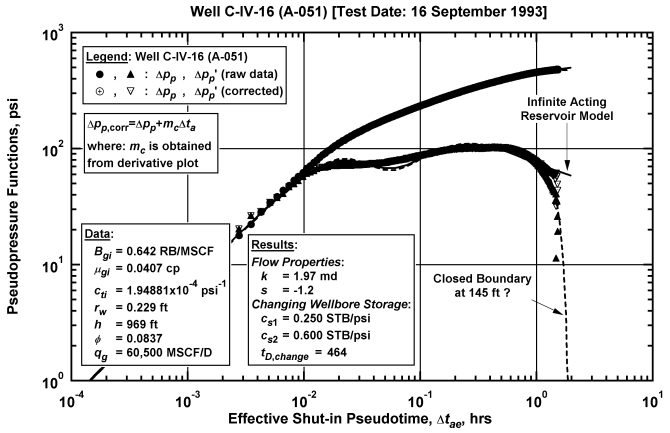

Fig. 28—Log-log plot of shut-in pseudopressure functions versus effective shut-in pseudotime for Well C-IV-16 (A-051) [16 September 1993].

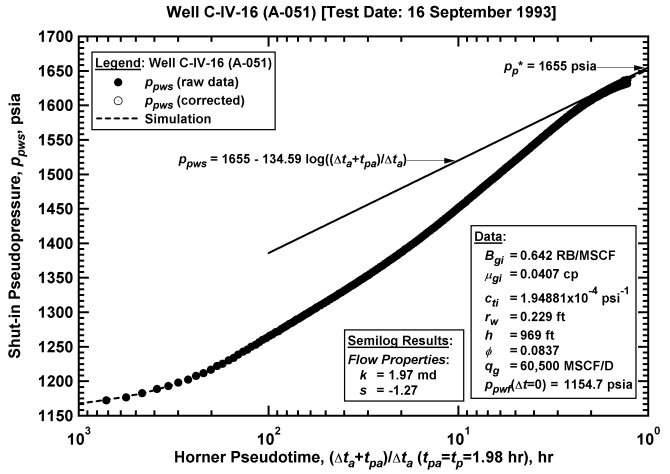

Fig. 29—Semilog plot of shut-in pseudopressure function versus shut-in pseudotime for Well C-IV-16 (A-051) [16 September 1993].

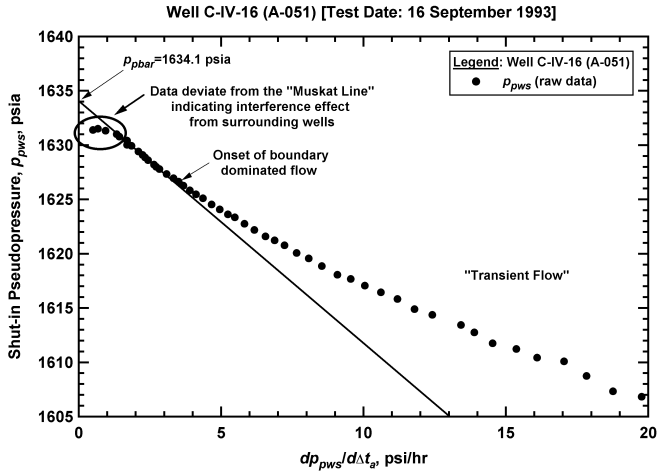

Fig. 30—Muskat plot for Well C-IV-16 (A-051) [16 September 1993].

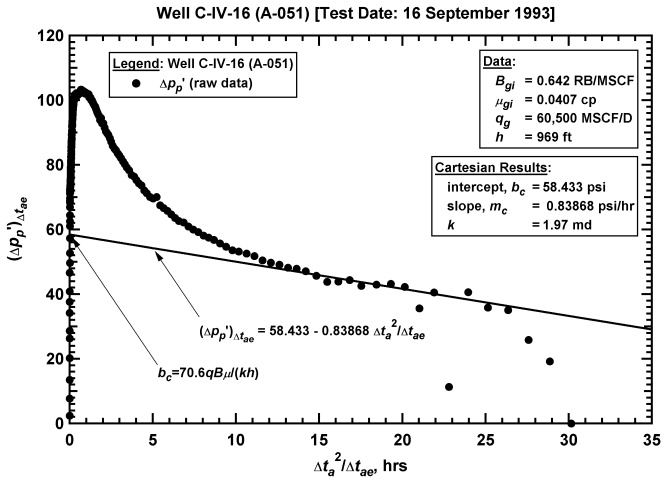

Fig. 31—Well Interference plot, Well C-IV-16 (A-051) [16 Sep 1993].